Amyloidogenic peptide oligomer accumulation in autophagy-deficient β cells induces diabetes

Jinyoung Kim,[1,2] Hwanju Cheon,[1] Yeon Taek Jeong,[1] Wenying Quan,[1] Kook Hwan Kim,[1] Jae Min Cho,[1] Yu-Mi Lim,[1] Seung Hoon Oh,[1] Sang-Man Jin,[1] Jae Hyeon Kim,[1] Moon-Kyu Lee,[1] Sunshin Kim,[3] Masaaki Komatsu,[4] Sang-Wook Kang,[5] and Myung-Shik Lee[1,2]

[1]Department of Medicine and [2]Samsung Advanced Institute for Health Sciences and Technology, Samsung Medical Center, Sungkyunkwan University School of Medicine, Seoul, Republic of Korea. [3]New Experimental Therapeutics Branch, Korean National Cancer Center, Goyang, Republic of Korea. [4]Department of Biochemistry, Niigata University School of Medicine, Niigata, Japan. [5]Department of Biomedical Sciences, University of Ulsan, Seoul, Republic of Korea.

Islet amyloid accumulation is a hallmark of human type 2 diabetes (T2D). In contrast to human islet amyloid polypeptide (hIAPP), murine islet amyloid polypeptide (mIAPP) does not exhibit amyloidogenic propensity. Because autophagy is important in the clearance of amyloid-like proteins, we studied transgenic mice with β cell–specific expression of *hIAPP* to evaluate the contribution of autophagy in T2D-associated accumulation of hIAPP. In mice with β cell–specific expression of *hIAPP*, a deficiency in autophagy resulted in development of overt diabetes, which was not observed in mice expressing *hIAPP* alone or lacking autophagy alone. Furthermore, lack of autophagy in *hIAPP*-expressing animals resulted in hIAPP oligomer and amyloid accumulation in pancreatic islets, leading to increased death and decreased mass of β cells. Expression of *hIAPP* in purified monkey islet cells or a murine β cell line resulted in pro-hIAPP dimer formation, while dimer formation was absent or reduced dramatically in cells expressing either nonamyloidogenic *mIAPP* or nonfibrillar mutant *hIAPP*. In autophagy-deficient cells, accumulation of pro-hIAPP dimers increased markedly, and pro-hIAPP trimers were detected in the detergent-insoluble fraction. Enhancement of autophagy improved the metabolic profile of *hIAPP*-expressing mice fed a high-fat diet. These results suggest that autophagy promotes clearance of amyloidogenic hIAPP, autophagy deficiency exacerbates pathogenesis of human T2D, and autophagy enhancers have therapeutic potential for islet amyloid accumulation-associated human T2D.

Introduction

Macroautophagy (hereafter referred to as autophagy) is characterized by the rearrangement of subcellular membranes to sequester cytoplasm and organelles for delivery to lysosomes, in which the sequestered material is degraded and recycled (1). Because autophagy degrades dysfunctional organelles and damaged proteins for rejuvenation of their function or retrieval of nutrients, autophagy plays important roles in the maintenance of intracellular homeostasis and physiological function of normal tissues (1). In addition to the physiological roles, dysregulated autophagy contributes to the pathogenesis of diverse disease processes, such as neurodegeneration, cancer, and metabolic disorders (2).

Type 2 diabetes (T2D) is a metabolic disorder characterized by an abnormal regulation of nutrients and their metabolites that develops as a consequence of combined insulin resistance and relative insulin deficiency (3). Recent investigations showed a close relationship between autophagy and the pathogenesis of T2D (4–8).

▶ Related Commentary: p. 3292

Authorship note: Jinyoung Kim, Hwanju Cheon, and Yeon Taek Jeong contributed equally to this work.
Conflict of interest: The authors have declared that no conflict of interest exists.
Submitted: March 18, 2013; **Accepted:** May 29, 2014.
Reference information: *J Clin Invest*. 2014;124(8):3311–3324. doi:10.1172/JCI69625.

We and others have reported that autophagy is important in the maintenance of pancreatic β cell mass and function (4, 5). Dysregulated autophagy in insulin target tissues has been associated with altered insulin sensitivity and lipid metabolism (6–8).

The mechanisms of β cell failure in T2D have been investigated extensively using animal models of T2D. However, T2D animal models may have limitations, in that disease pathogenesis or course might be different in several respects between murine and human T2D. One of the fundamental differences is the frequent deposition of amyloid in islets of humans with T2D. Due to the fact that human islet amyloid polypeptide (hIAPP), the major component of islet amyloid, is amyloidogenic, while the murine form is not, islet amyloid is found in up to 90% of individuals with T2D at autopsy but not in murine T2D (9). Such a difference in the propensity to form amyloid is due to the difference in the amino acid sequences of islet amyloid polypeptide (IAPP) (10). It has been suggested that aggregate-prone or amyloid-like proteins are cleared preferentially by autophagy, while proteasomal degradation is a critical part of the clearance of nonaggregate-prone proteins (11). Hence, autophagy seems to be more important for the removal of amyloidogenic hIAPP compared with mouse islet amyloid polypeptide (mIAPP), and dysregulated autophagy may be more relevant to the pathogenesis of human T2D rather than that of murine T2D.

While murine T2D models are not suitable for the study of amyloidogenic IAPP, transgenic mice expressing *hIAPP* specifically in pancreatic β cells (*hIAPP*$^+$ mice) could serve as a surrogate

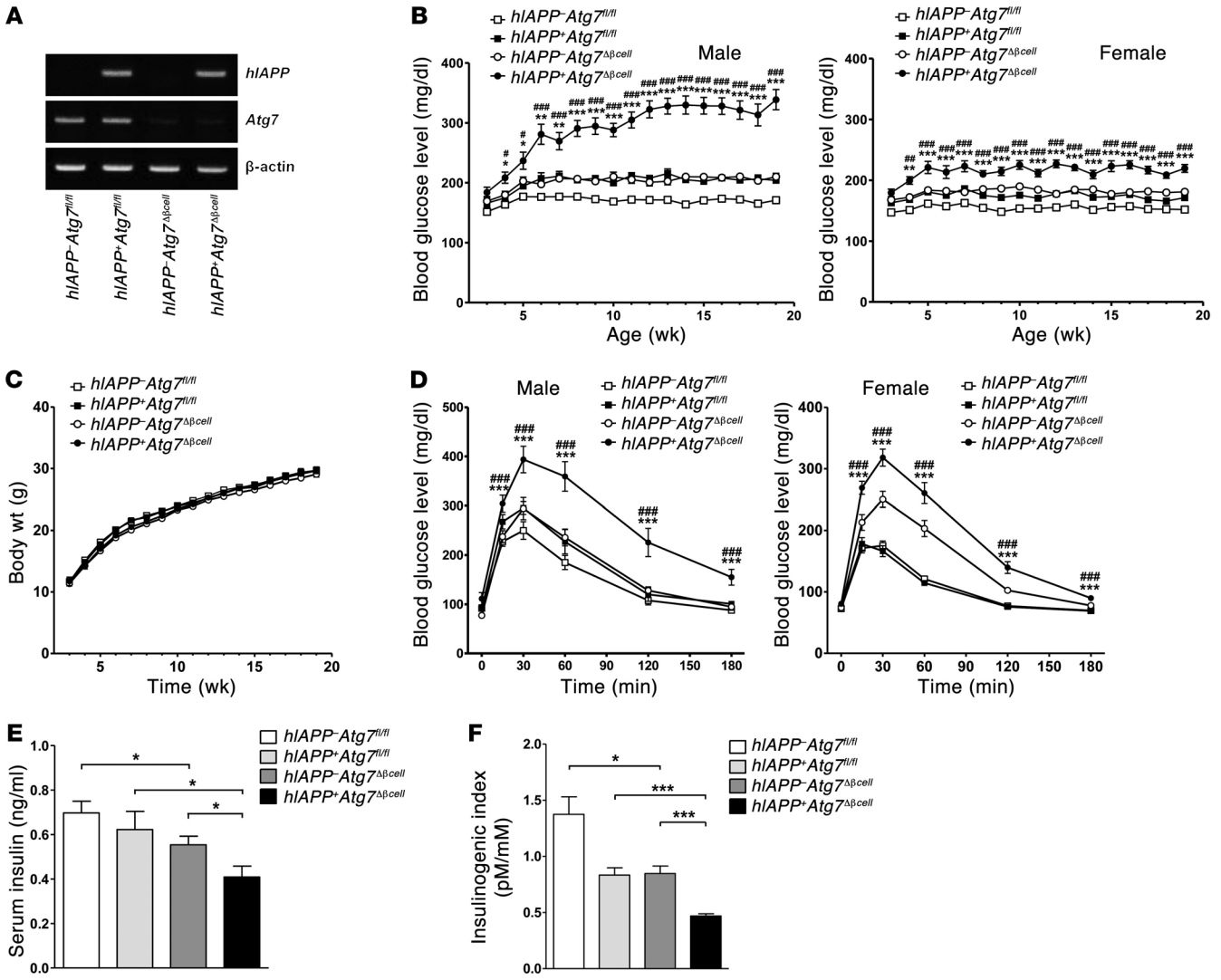

Figure 1. Development of diabetes in *hIAPP⁺Atg7^Δβcell* mice. (**A**) RT-PCR analysis of *hIAPP* and *Atg7* expression in primary islets. The residual expression of *Atg7* in islets of *hIAPP⁻Atg7^Δβcell* or *hIAPP⁺Atg7^Δβcell* mice is probably due to non–β cells in primary islets. (**B**) Nonfasting blood glucose levels in male and female mice (n = 33~46 for male and 30~51 for female mice between 8 and 20 week of age; n = 10~16 for male and 10~19 for female mice before 8 weeks of age). (**C**) Body weight of male mice. Body weight of female mice was also not different between groups (data not shown). The numbers of mice in **C** are the same as those in **B**. (**D**) IPGTT after overnight fasting in 12- to 15-week-old male (n = 5~7) and female mice (n = 12~23). (**E**) Serum insulin levels in fasted 12- to 15-week-old male mice determined by ELISA (n = 10 each). (**F**) The insulinogenic index was calculated from 12- to 15-week-old male mice (n = 5~7). $^{*}P < 0.05$, $^{**}P < 0.01$, $^{***}P < 0.001$; $^{\#}P < 0.05$, $^{\#\#}P < 0.01$, $^{\#\#\#}P < 0.001$. (*, comparison with *hIAPP⁺Atg7^fl/fl* mice; #, comparison with *hIAPP⁻Atg7^Δβcell* mice in **B** and **D**.)

animal model to study the role of autophagy in the clearance of amyloidogenic IAPP in human T2D (12–15). We produced *hIAPP*⁺ mice with β cell–specific autophagy deficiency and investigated the role of autophagy in the development of diabetes associated with the accumulation of hIAPP.

Results

Development of diabetes in hIAPP⁺ mice with β cell–specific autophagy deficiency. We bred RIP-*Cre* mice expressing Cre recombinase in pancreatic β cells with *Atg7*-floxed mice (*Atg7^fl/fl* mice) and crossed them with *hIAPP*⁺ mice expressing *hIAPP* specifically in β cells (13) to ultimately derive heterozygous *hIAPP*⁺ mice with β cell–specific *Atg7* deficiency (*hIAPP⁺Atg7^fl/fl^Cre⁺* mice, hereafter referred to as *hIAPP⁺Atg7^Δβcell* mice). When we conducted RT-PCR using mRNA from pancreatic islets of these mice, *hIAPP* expression was observed, while the expression of *Atg7* was negligible (Figure 1A).

Intriguingly, male *hIAPP⁺Atg7^Δβcell* mice developed overt diabetes beginning at 6 weeks of age (Figure 1B), while male littermate autophagy-competent *hIAPP*⁺ mice (*hIAPP⁺Atg7^fl/fl^Cre⁻* mice, hereafter referred to as *hIAPP⁺Atg7^fl/fl* mice) or *hIAPP*⁻ mice with β cell–specific *Atg7* deficiency (*hIAPP⁻Atg7^fl/fl^Cre⁺* mice, hereafter referred to as *hIAPP⁻Atg7^Δβcell* mice) did not develop diabetes through 1 year of age, consistent with previous papers (5, 13). Female *hIAPP⁺Atg7^Δβcell* mice did not develop overt diabetes; however, nonfasting blood glucose levels of female *hIAPP⁺Atg7^Δβcell* mice were significantly higher than those of female *hIAPP⁺Atg7^fl/fl* or *hIAPP⁻Atg7^Δβcell* mice (P < 0.01~0.001) (Figure 1B). Body weight did not differ among groups in either male or female mice (P > 0.1) (Fig-

ure 1C and data not shown). An i.p. glucose tolerance test (IPGTT) showed more severe glucose intolerance in male and female *hIAPP*$^{+}$*Atg7*$^{\Delta\beta cell}$ mice compared with that in male and female *hIAPP*$^{+}$*Atg7*$^{fl/fl}$ or *hIAPP*$^{-}$*Atg7*$^{\Delta\beta cell}$ mice, respectively ($P < 0.001$) (Figure 1D).

Since diabetes was overt only in male *hIAPP*$^{+}$*Atg7*$^{\Delta\beta cell}$ mice, subsequent studies were conducted using male *hIAPP*$^{+}$*Atg7*$^{\Delta\beta cell}$ mice. The fasting serum insulin level and insulinogenic index representing β cell function (16) were significantly lower in *hIAPP*$^{+}$*Atg7*$^{\Delta\beta cell}$ mice compared with those in *hIAPP*$^{+}$*Atg7*$^{fl/fl}$ or *hIAPP*$^{-}$*Atg7*$^{\Delta\beta cell}$ mice ($P < 0.05$~0.001) (Figure 1, E and F), suggesting that insulin deficiency due to the synergistic effect of autophagy deficiency and *hIAPP* expression is responsible for the development of overt diabetes in *hIAPP*$^{+}$*Atg7*$^{\Delta\beta cell}$ mice.

Changes of β cell mass and function in hIAPP^{+}*Atg7*$^{\Delta\beta cell}$ *mice*. We next conducted morphological analysis of pancreatic islets in *hIAPP*$^{+}$*Atg7*$^{\Delta\beta cell}$ mice. Microscopic examination after H&E staining revealed frequent vacuolar degeneration and cells with areas of detachment from surrounding cells or tissues in islets of *hIAPP*$^{+}$*Atg7*$^{\Delta\beta cell}$ mice (Figure 2A). These changes appeared morphologically similar to, but apparently more severe, than those of *hIAPP*$^{-}$*Atg7*$^{\Delta\beta cell}$ mice (5). Individual cell counting revealed that a significantly increased number of cells was detached from surrounding cells or tissues in islets of *hIAPP*$^{+}$*Atg7*$^{\Delta\beta cell}$ mice compared with that in *hIAPP*$^{-}$*Atg7*$^{\Delta\beta cell}$ or *hIAPP*$^{+}$*Atg7*$^{fl/fl}$ mice ($P < 0.05$~0.001) (Figure 2A). Some of the vacuolated cells contained nuclei with chromatin condensation or did not contain nuclei, suggesting apoptosis. Accumulation of ubiquitin and p62 that was seen in islets of *Atg7*$^{\Delta\beta cell}$ mice due to autophagy deficiency (5) was also observed in islets of *hIAPP*$^{+}$*Atg7*$^{\Delta\beta cell}$ mice (Figure 2B). Confocal microscopy showed that ubiquitin and p62 were colocalized, similar to the finding in *hIAPP*$^{-}$*Atg7*$^{\Delta\beta cell}$ mice (ref. 5 and Figure 2B). p62 or ubiquitin accumulation was not detected in *hIAPP*$^{+}$*Atg7*$^{fl/fl}$ mice (Figure 2B).

β Cell mass measured by point counting after insulin immunohistochemistry (IHC) was not different between *hIAPP*$^{+}$*Atg7*$^{fl/fl}$ and *hIAPP*$^{-}$*Atg7*$^{fl/fl}$ mice, suggesting that heterozygous expression of *hIAPP* alone does not significantly affect β cell mass if autophagy is intact (Figure 2C). In *hIAPP*$^{+}$*Atg7*$^{\Delta\beta cell}$ mice, however, β cell mass was further reduced compared with that in *hIAPP*$^{-}$*Atg7*$^{\Delta\beta cell}$ mice ($P < 0.01$), which already had a significantly lower β cell mass compared with autophagy-competent *hIAPP*$^{-}$*Atg7*$^{fl/fl}$ mice ($P < 0.05$) (Figure 2C).

Since these findings suggested that markedly reduced pancreatic β cell mass is the cause of insulin deficiency and overt diabetes in *hIAPP*$^{+}$*Atg7*$^{\Delta\beta cell}$ mice, we next conducted TUNEL staining to study the mechanism underlying the reduced β cell mass in *hIAPP*$^{+}$*Atg7*$^{\Delta\beta cell}$ mice. While only modestly increased numbers of apoptotic cells were observed in islets of *hIAPP*$^{+}$*Atg7*$^{fl/fl}$ or *hIAPP*$^{-}$*Atg7*$^{\Delta\beta cell}$ mice, the number of apoptotic β cells was markedly increased in *hIAPP*$^{+}$*Atg7*$^{\Delta\beta cell}$ mice compared with that in *hIAPP*$^{+}$*Atg7*$^{fl/fl}$ or *hIAPP*$^{-}$*Atg7*$^{\Delta\beta cell}$ mice ($P < 0.01$~0.001) (Figure 2D), indicating that increased pancreatic β cell apoptosis is responsible for the critically reduced β cell mass in *hIAPP*$^{+}$*Atg7*$^{\Delta\beta cell}$ mice.

We also studied pancreatic β cell function by investigating Ca^{2+} transients after glucose challenge. Consistent with a previous report (5), the magnitude of glucose-induced Ca^{2+} transients was significantly reduced in autophagy-deficient β cells from *hIAPP*$^{-}$*Atg7*$^{\Delta\beta cell}$ mice compared with that in cells from control *hIAPP*$^{-}$*Atg7*$^{fl/fl}$ mice, as shown by the suppressed area of the change in cytosolic free Ca^{2+} concentration ($\Delta[Ca^{2+}]_c$) above basal cytosolic free Ca^{2+} concentration ($[Ca^{2+}]_c$), ($P < 0.01$) (Figure 2, E and F). Glucose-induced Ca^{2+} transients and $\Delta[Ca^{2+}]_c$ area appeared to be decreased in islets from *hIAPP*$^{+}$*Atg7*$^{fl/fl}$ mice compared with wild-type islets; however, the difference was not statistically significant ($P > 0.1$) (Figure 2, E and F). Intriguingly, in islets from *hIAPP*$^{+}$*Atg7*$^{\Delta\beta cell}$ mice, glucose-induced Ca^{2+} transients and $\Delta[Ca^{2+}]_c$ area were further suppressed compared with those from *hIAPP*$^{-}$*Atg7*$^{\Delta\beta cell}$ or *hIAPP*$^{+}$*Atg7*$^{fl/fl}$ mice ($P < 0.05$~0.01) (Figure 2, E and F). Together with the elevated level of basal $[Ca^{2+}]_c$ in islets from *hIAPP*$^{+}$*Atg7*$^{\Delta\beta cell}$ mice, which supports β cell dysfunction (Figure 2E), these findings suggest that mild functional impairment by hIAPP is aggravated if autophagy is deficient and that the combination of decreased β cell mass and impaired β cell function is responsible for markedly reduced insulin release and severe diabetes in *hIAPP*$^{+}$*Atg7*$^{\Delta\beta cell}$ mice.

Accumulation of hIAPP oligomer and amyloid in islets of hIAPP^{+}*Atg7*$^{\Delta\beta cell}$ *mice*. We attempted to determine the possible presence of intracellular hIAPP oligomer in autophagy-deficient β cells using I11 Ab that was raised against hIAPP oligomer or A11 Ab that was raised against Aβ42 fibril but recognizes hIAPP oligomer (17), because oligomer of amyloidogenic hIAPP peptide rather than mature hIAPP amyloid or hIAPP monomer is considered to be a major effector of cellular damages (18). When we conducted confocal microscopy after immunofluorescent staining using I11 Ab as the primary Ab, hIAPP oligomer was not detected in islets of *hIAPP*$^{-}$*Atg7*$^{\Delta\beta cell}$ mice as expected. hIAPP oligomer was virtually absent in pancreatic islets of autophagy-competent 12-week-old male *hIAPP*$^{+}$*Atg7*$^{fl/fl}$ mice, except in a few scattered areas, suggesting that hIAPP oligomer was not formed or was rapidly processed by autophagy and/or other types of intracellular proteolysis, leaving no detectable amount of hIAPP oligomer (Figure 3A). In contrast, prominent hIAPP oligomer accumulation was detected in pancreatic islets of 12-week-old *hIAPP*$^{+}$*Atg7*$^{\Delta\beta cell}$ mice (Figure 3A), indicating the formation and accumulation of hIAPP oligomer. Confocal microscopy showed that hIAPP oligomer detected by I11 Ab in pancreatic islets of *hIAPP*$^{+}$*Atg7*$^{\Delta\beta cell}$ mice was largely colocalized with insulin, suggesting that hIAPP oligomer is located inside β cells (Figure 3A). hIAPP oligomer that was not colocalized with insulin was also observed, probably due to reduced insulin production in damaged β cells as a result of the combination of hIAPP oligomer accumulation and autophagy deficiency. Confocal microscopy showed that I11-stained hIAPP oligomer was not colocalized with p62, except in a few areas (Figure 3B).

Because these results suggested that hIAPP oligomer accumulates in autophagy-deficient β cells and autophagy plays an important role in the clearance of hIAPP oligomer, we next sought morphological evidence supporting autophagy-mediated clearance of hIAPP oligomer by studying colocalization of hIAPP oligomer and autophagosomes. To this end, we used homozygous *hIAPP*-transgenic mice (*hIAPP*$^{+/+}$ mice), because colocalization of hIAPP oligomer and autophagosomes is not possible using *hIAPP*$^{+}$*Atg7*$^{\Delta\beta cell}$ mice that have autophagy deficiency in β cells or *hIAPP*$^{+}$*Atg7*$^{fl/fl}$ mice that show virtually no accumulation of hIAPP oligomer (Figure 3A). We produced *hIAPP*$^{+/+}$*GFP-LC3*$^{+}$ mice by breeding *GFP-LC3*$^{+}$ mice, which have been used widely

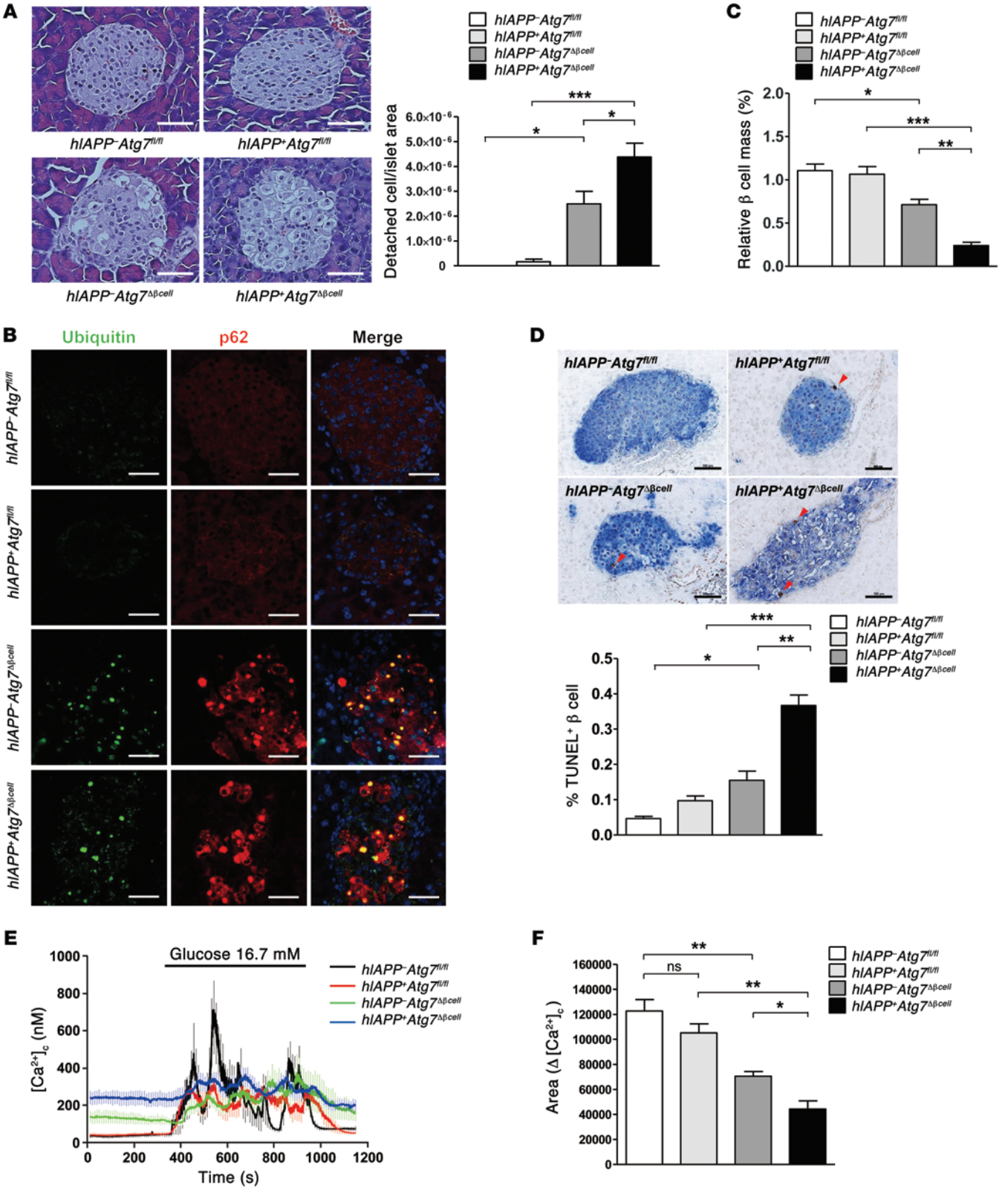

Figure 2. β Cells in *hIAPP⁺Atg7^Δβcell* mice. (**A**) H&E staining of pancreas sections and the number of cells detached from surrounding tissues or cells per islet area in 12- to 15-week-old mice (n = 3~6). Scale bar: 100 μm. (**B**) Confocal microscopy after immunofluorescent staining of pancreas sections from 12- to 15-week-old mice using anti-p62 and -ubiquitin Abs. Scale bar: 100 μm. (**C**) Relative β cell mass in 12- to 15-week-old mice measured by insulin IHC and the point counting method (n = 3 each). (**D**) The percentage of apoptotic TUNEL⁺ β cells among total β cells in islets of 12- to 15-week-old mice (n = 4~5). Representative TUNEL staining is shown. Arrowheads indicate TUNEL⁺ β cells. Scale bar: 100 μm. (**E**) Glucose-induced Ca^{2+} transients in isolated islets (n = 4 each). Ca^{2+} transients were measured in Tyrode solution containing 3.0 or 16.7 mM glucose, as described in the Methods. (**F**) $\Delta[Ca^{2+}]_c$ area was defined as the total area of $[Ca^{2+}]_c$ above basal $[Ca^{2+}]_c$. $^*P < 0.05$, $^{**}P < 0.01$, $^{***}P < 0.001$. ns, not significant.

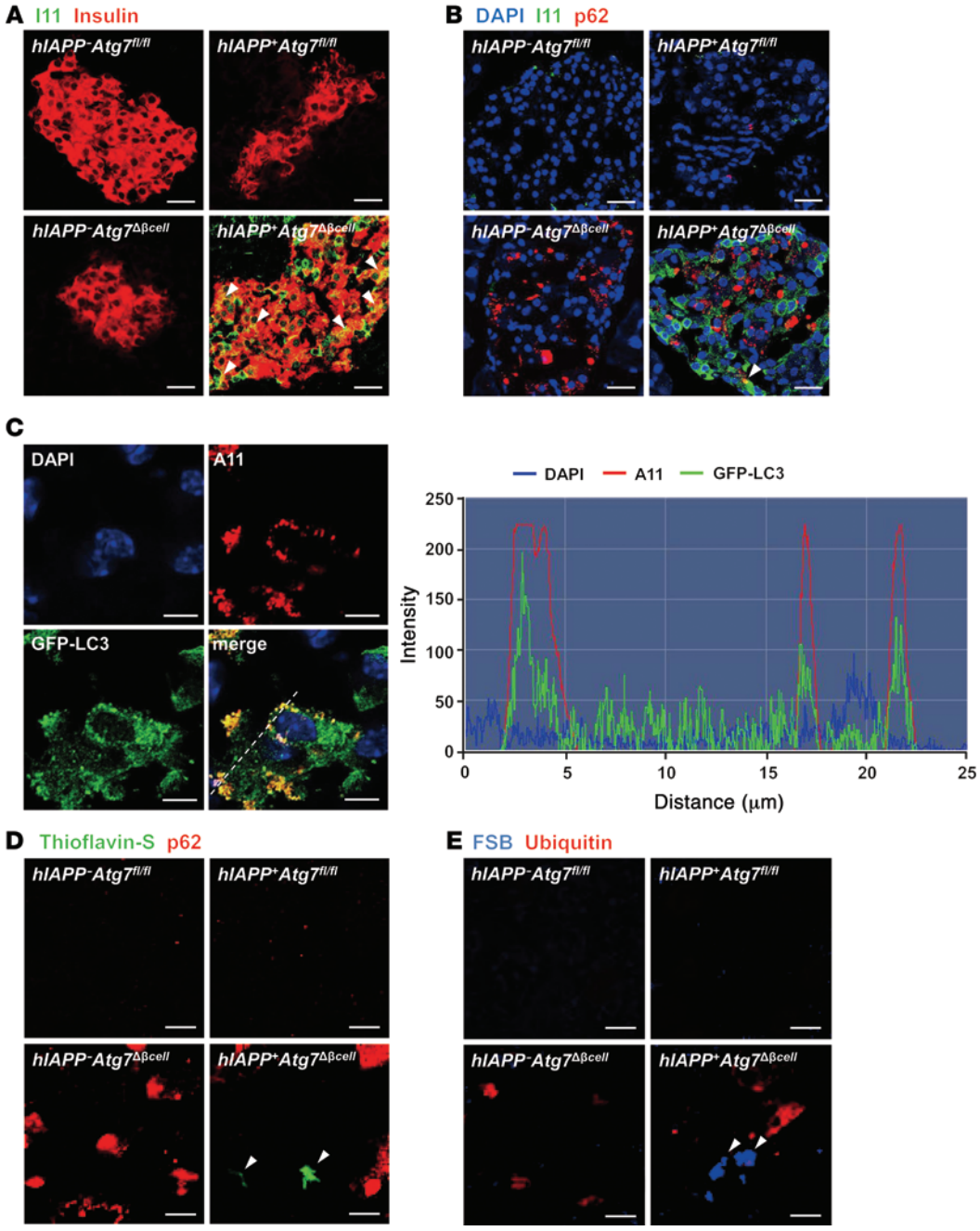

Figure 3. In vivo accumulation of hIAPP oligomer and amyloid. (**A**) Confocal microscopy after immunofluorescent staining of pancreas sections from 12-week-old mice using anti-insulin and anti-hIAPP oligomer Abs (I11). Arrowheads indicate colocalization of I11 and insulin immunostaining. Scale bar: 50 μm. (**B**) Confocal microscopy after immunofluorescent staining using anti-p62 and I11 Ab and subsequent DAPI staining to identify nuclei. The arrowhead indicates rare colocalization of I11 and p62 immunostaining. Scale bar: 50 μm. (**C**) Confocal microscopy after immunofluorescent staining of *hIAPP*$^{+/+}$*GFP-LC3*$^{+}$ mouse islets using A11 Ab. Line tracing performed along the white dashed line in the merged picture to visualize colocalization of A11-stained hIAPP oligomer and *GFP-LC3*$^{+}$ autophagosomes shows overlapping of hIAPP fluorescence with GFP fluorescence. Scale bar: 5 μm. (**D** and **E**) Confocal microscopy after immunofluorescent staining of pancreas sections from 12-week-old mice using (**D**) anti-p62 Ab and thioflavin-S staining or (**E**) using anti-ubiquitin Ab and FSB staining, as described in the Methods. Arrowheads indicate amyloid stained with thioflavin-S (green) or FSB (blue). Scale bar: 5 μm.

to visualize autophagosomes (19), with *hIAPP*$^{+}$ mice twice to make *hIAPP* homozygotes expressing *GFP-LC3*. Accumulation of hIAPP oligomer stained with A11 Ab was observed in islet cells of *hIAPP*$^{+/+}$*GFP-LC3*$^{+}$ mice by confocal microscopy, consistent with previous results (ref. 20 and Figure 3C). Confocal microscopy and line tracing showed that hIAPP oligomer was colocalized with GFP-LC3 puncta representing autophagosomes in pancreatic islets of *hIAPP*$^{+/+}$*GFP-LC3*$^{+}$ mice (Figure 3C), suggesting that hIAPP oligomer makes contact with autophagosome and is probably cleared by autophagy.

In addition to hIAPP oligomer, we also studied possible accumulation of amyloid in pancreatic islets. Thioflavin-S staining, a classical method to detect amyloid, demonstrated that hIAPP amyloid accumulated in pancreatic islets of 12-week-old *hIAPP*$^{+}$*Atg7*$^{\Delta\beta cell}$ mice but not in other types of mice (Figure 3D). Confocal microscopy showed that hIAPP amyloid was not colocalized with inclusion bodies containing p62 (Figure 3D). Staining with EE-1-fluoro-2,5-bis(3-hydroxycarbonyl-4-hydroxy)styrylbenzene (FSB), another amyloid-specific dye that was developed as a lipophilic derivative of Congo Red (21, 22), again showed that mature hIAPP amyloid, while small in size, was formed and scattered in pancreatic islets of *hIAPP*$^{+}$*Atg7*$^{\Delta\beta cell}$ mice (Figure 3E), substantiating our results using thioflavin-S. FSB-stained amyloid was not observed in islets of *hIAPP*$^{+}$*Atg7*$^{fl/fl}$ or *hIAPP*$^{-}$*Atg7*$^{\Delta\beta cell}$ mice. FSB staining in *hIAPP*$^{+}$*Atg7*$^{\Delta\beta cell}$ mice was not colocalized with ubiquitin-containing inclusion bodies (Figure 3E).

Accumulation of IAPP oligomer in vitro. Since hIAPP oligomer accumulates in autophagy-deficient β cells in vivo and probably

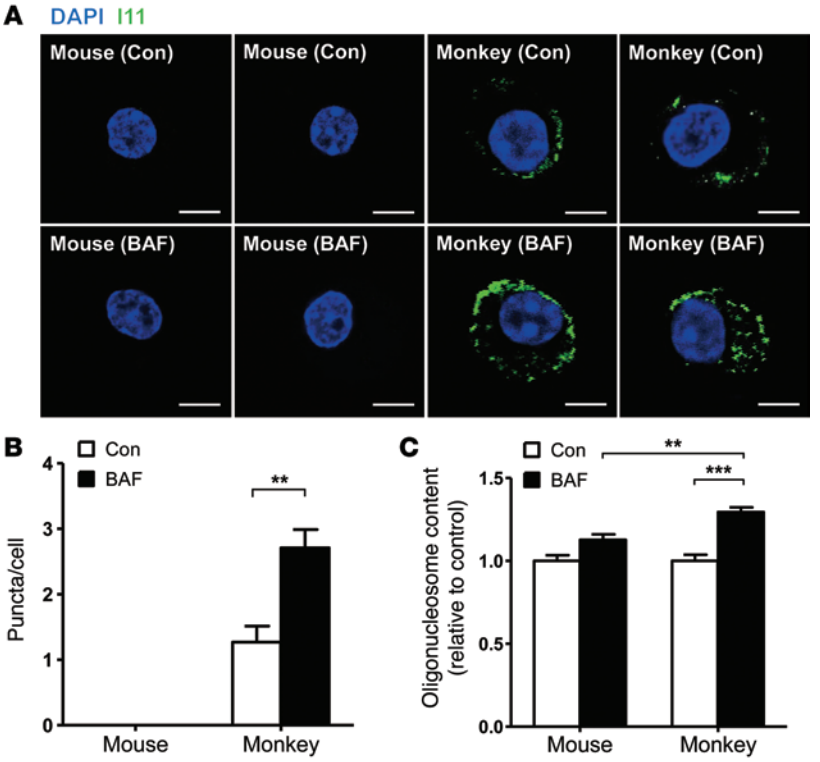

Figure 4. Accumulation of I11-stained IAPP oligomer in primary monkey islet cells. (**A**) Primary monkey islet cells or mouse islet cells were incubated with 100 nM bafilomycin (BAF) that efficiently blocks autophagy of primary cells or solvent alone (Con) for 24 hours. Confocal microscopy was performed after immunofluorescent staining using I11 Ab. Scale bar: 5 μm. (**B**) The number of I11-stained puncta was counted. (**C**) After the same incubation of primary monkey and mouse islet cells with or without bafilomycin, apoptosis was determined by measuring oligonucleosomal content in cell extract using a Cell Death Detection ELISA Kit (Roche). $^{**}P < 0.01$, $^{***}P < 0.001$.

leads to β cell apoptosis, we next studied whether similar findings occur in vitro. We prepared primary islet cells from monkeys expressing amyloidogenic IAPP that is almost identical to hIAPP (23) and incubated them with 100 nM bafilomycin for 24 hours to inhibit autophagic degradation of endogenous monkey IAPP. Immunostaining showed accumulation of I11-stained IAPP oligomer in monkey islet cells, which was increased by incubation with bafilomycin ($P < 0.01$) (Figure 4, A and B). I11-stained IAPP oligomer was not detected in primary mouse islet cells cultured and treated in the same way. When assessed by measuring cytoplasmic oligonucleosome, apoptosis of primary monkey islet cells after treatment with bafilomycin was more pronounced than that of mouse islet cells, probably because of endogenous IAPP oligomer accumulation ($P < 0.01$) (Figure 4C), which is in line with the increased β cell apoptosis associated with I11-stained hIAPP oligomer accumulation in *hIAPP*$^{+}$*Atg7*$^{\Delta\beta cell}$ mouse islets in vivo (Figure 2D and Figure 3A). However, amyloid accumulation was not observed after incubation of primary monkey islet cells with bafilomycin for 24 hours (Supplemental Figure 1; supplemental material available online with this article; doi:10.1172/JCI69625DS1).

Detection of pro-hIAPP dimer and trimer in islet cells. Because these results suggested that increased accumulation of toxic hIAPP oligomer in autophagy deficiency leads to β cell apoptosis and diabetes, we investigated which kinds of hIAPP oligomers accumulate in association with β cell autophagy deficiency. To this end, we overexpressed constructs encoding either mouse or human prepro-IAPP fused with HA epitope sequence at the C terminus (Figure 5A), since the unprocessed form of pro-hIAPP rather than mature hIAPP might be the initial seed for further fibril and amyloid formation (24–26) and an HA tag would facilitate detection of pro-hIAPP oligomers of varying sizes. Western blot analysis indicated that the majority of pro-IAPP expressed in INS-1 insulinoma cells transfected with prepro-IAPP-HA is a monomeric form of pro-hIAPP or pro-mIAPP (Figure 5B). Intriguingly, a minor species of pro-IAPP, which is larger in size than the monomeric form, was additionally observed in cells transfected with prepro-hIAPP but not in cells transfected with prepro-mIAPP construct and was markedly increased in cells incubated with 5 mM 3-MA, a potent inhibitor of autophagy (Figure 5B). Estimation of the size suggested that this band is a dimeric form of pro-hIAPP; this was substantiated by the remarkable reduction of this species in cells expressing a nonfibrillar mutant form of *hIAPP* (prepro-hIAPP^{mt}) (ref. 27 and Figure 5, A and C), and its C-terminal HA epitope was still detectable with anti-HA Ab (Figure 5A). This band was not a product of incomplete cleavage of the signal peptide from prepro-hIAPP, because the size of uncleaved prepro-hIAPP produced by the site-directed mutagenesis of the cleavage site (28) was apparently smaller than that of the putative pro-hIAPP dimer (Supplemental Figure 2).

Additional evidence supporting the notion that pro-hIAPP oligomer accumulates in autophagy-deficient cells was provided by the observation that, not only the dimeric, but also the trimeric form of pro-hIAPP was recovered in the detergent-insoluble fraction of cells treated with 3-MA (Figure 5D). pro-hIAPP trimer was not observed in cells not treated with 3-MA or in the detergent-soluble fraction of cells treated with 3-MA (Figure 5D). Although it remains to be clarified which types of pro-hIAPP oligomers are preferred autophagic substrates, our results clearly show that the immature or unprocessed form of fibril-prone pro-hIAPP selectively oligomerizes and accumulates in autophagy-deficient cells, which could be the initial step in the formation of islet amyloid.

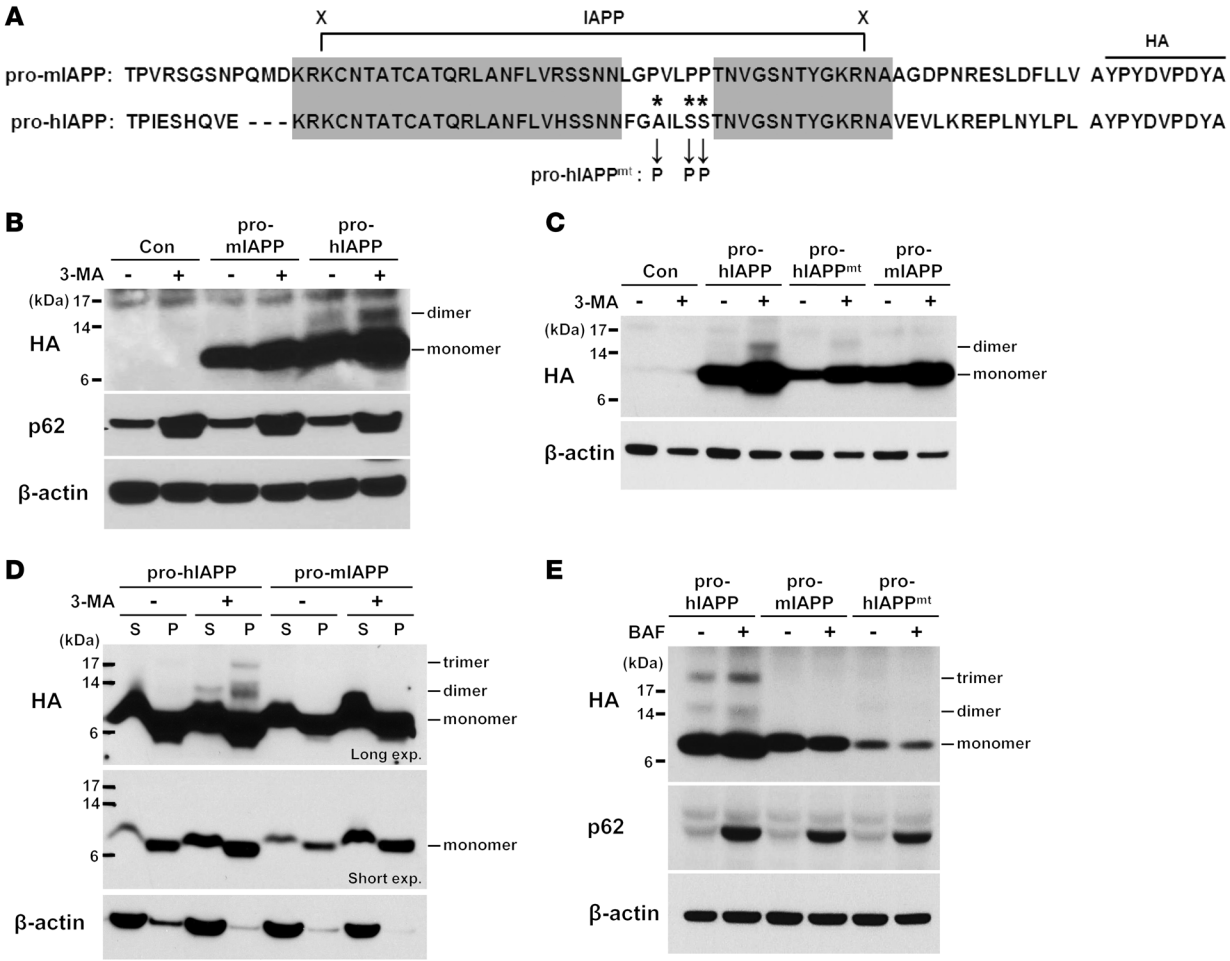

Figure 5. Pro-hIAPP dimer and trimer. (**A**) Amino acid sequences of pro-IAPP used in this study. The highly conserved region between hIAPP and mIAPP is indicated in gray boxes. Cleavage sites of proprotein convertase 2 (left) and 1/3 (right) are indicated with "X"s. Asterisks indicate mutation sites in which the original amino acids were changed to prolines in pro-hIAPP^{mt}. (**B**) INS-1 cells were transfected with indicated constructs for 24 hours and incubated with or without 5 mM 3-MA for additional 24 hours. Cell lysates were subjected to Western blot analysis using anti-HA Ab. Equal protein loading and autophagy inhibition were confirmed by β-actin and p62 levels, respectively. (**C**) After transfection of INS-1 cells with indicated constructs and treatment with 3-MA as in **B**, cell lysates were prepared and subjected to Western blot analysis. (**D**) INS-1 cells were transfected and treated as in **B**. The detergent-soluble (S) and detergent-insoluble (P) pellet fractions were subjected to Western blot analysis using anti-HA Ab. Equal protein loading was confirmed by β-actin level. Differential migration of monomeric pro-IAPPs between detergent-soluble and -insoluble fractions was due to the difference in the detergents used. exp., exposure. (**E**) Primary monkey islet cells were transfected with the indicated constructs for 24 hours and incubated with or without 100 nM bafilomycin for an additional 24 hours. Cell lysates were subjected to Western blot analysis using anti-HA Ab. Equal protein loading and autophagy inhibition were confirmed by β-actin and p62 level, respectively.

We next studied whether the pro-hIAPP dimer or trimer could accumulate in primary islet cells as well, since insulinoma cells may have a diminished capacity to process proinsulin or pro-IAPP, which may cause erroneous accumulation of pro-hIAPP oligomer (24). When we transfected primary monkey islet cells with prepro-hIAPP-HA, pro-hIAPP dimer and trimer accumulation was again observed by Western blot analysis using anti-HA antibody, which was not detected when prepro-mIAPP-HA construct was transfected (Figure 5E). Accumulation of pro-hIAPP dimer or trimer was much increased when primary monkey islet cells were incubated with 100 nM bafilomycin, which efficiently inhibits autophagy of primary islet cells (Figure 5E). These results indicate that pro-hIAPP dimer and trimer accumulation due to autophagy inhibition occurs in primary islet cells as well as in insulinoma cells and that pro-hIAPP dimer and trimer accumulation in INS-1 cells is not due to diminished pro-hIAPP processing in insulinoma cells.

Effect of hIAPP on autophagy. Because these data suggested that clearance of amyloidogenic proteins is modulated by autophagy status, we conversely studied whether autophagy is affected by hIAPP, an amyloidogenic protein. We again used homozygous *hIAPP*$^{+/+}$ or *hIAPP*$^{+/+}$*GFP-LC3*$^{+}$ mice that expressed double doses of the *hIAPP* transgene and showed hIAPP oligomer accumulation in islet cells as compared with those from heterozygous *hIAPP*$^{+}$ mice without detectable hIAPP accumulation (Figure 3, A and C). Immunofluorescent microscopy clearly showed LC3 puncta in pancreatic islet cells of *hIAPP*$^{+/+}$*GFP-LC3*$^{+}$ mice, while they were rarely observed in littermate *hIAPP*$^{-}$*GFP-LC3*$^{+}$ mice, suggesting that the steady-state autophagy level was increased by *hIAPP* transgene expression (Supplemental Figure 3A). EM also showed a significantly increased number of autophagosomes in islets of *hIAPP*$^{+/+}$ mice compared with that in *hIAPP*$^{-}$ mice ($P < 0.01$) (Supplemental Figure 3, B and C), again indicating increased

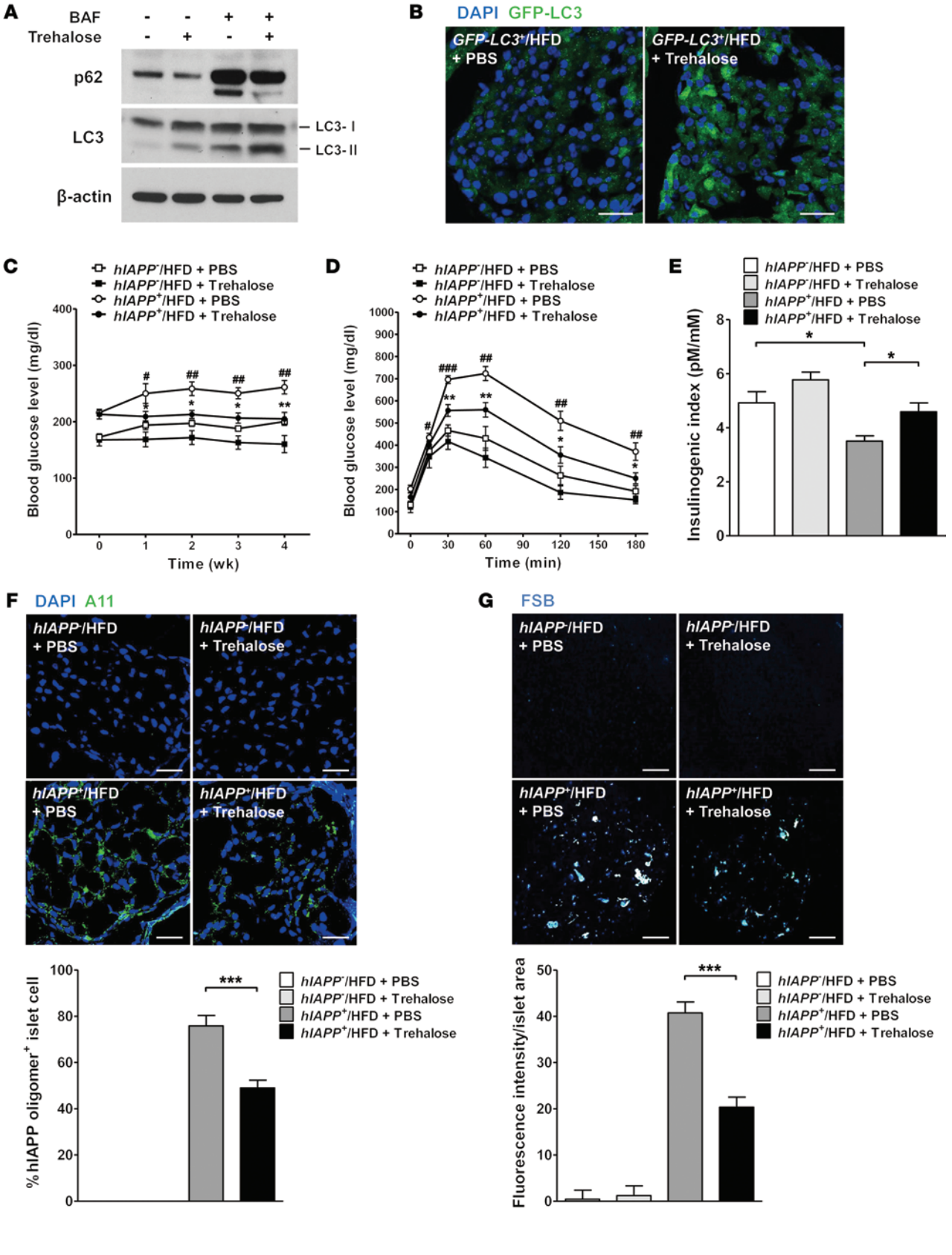
A
BAF
Trehalose
p62
LC3
LC3- I
LC3- II
β-actin
B
DAPI GFP-LC3
GFP-LC3+/HFD + PBS
GFP-LC3+/HFD + Trehalose
C
hIAPP-/HFD + PBS
hIAPP-/HFD + Trehalose
hIAPP+/HFD + PBS
hIAPP+/HFD + Trehalose
Blood glucose level (mg/dl)
Time (wk)
D
Blood glucose level (mg/dl)
Time (min)
E
Insulinogenic index (pM/mM)
F
DAPI A11
hIAPP-/HFD + PBS
hIAPP-/HFD + Trehalose
hIAPP+/HFD + PBS
hIAPP+/HFD + Trehalose
% hIAPP oligomer+ islet cell
G
FSB
Fluorescence intensity/islet area

Figure 6. Effects of autophagy enhancer on the glucose profile of hIAPP$^+$ mice. (**A**) Primary mouse islet cells were treated with 100 mM trehalose for 24 hours with or without 100 nM bafilomycin pretreatment to block lysosomal steps of autophagy. Cell lysates were subjected to Western blot analysis using anti-LC3 or anti-p62 Ab. (**B**) Trehalose (2 g/kg) was administered i.p. to 12-week-old *GFP-LC3*$^+$ mice on HFD for 2 weeks, and frozen pancreas sections were prepared for confocal microscopy to examine LC3 puncta. Scale bar: 50 μm. (**C**) Trehalose (2 g/kg) was administered i.p. to 16- to 20-week-old *hIAPP*$^+$ mice on HFD, and nonfasting blood glucose levels were monitored (n = 5). (**D**) IPGTT was performed after 4 weeks of trehalose administration to *hIAPP*$^+$ mice on HFD (n = 5). (**E**) The insulinogenic index was calculated after 4 weeks of trehalose administration to *hIAPP*$^+$ mice on HFD (n = 3). (**F**) After immunofluorescent staining using A11 Ab, the percentage of A11-stained cells among total DAPI$^+$ islet cells was determined by confocal microscopy. Representative pictures are shown. Scale bar: 50 μm. (**G**) After FSB staining, mean fluorescence intensity per islet area was determined using the NIS-Elements AR 3.0 software (Nikon). Representative pictures are shown. Scale bar: 100 μm. $^*P < 0.05$, $^{**}P < 0.01$, $^{***}P < 0.001$; $^{\#}P < 0.05$, $^{\#\#}P < 0.01$, $^{\#\#\#}P < 0.001$. (*, comparison between *hIAPP*$^+$/HFD + trehalose and *hIAPP*$^+$/HFD + PBS groups; #, comparison between *hIAPP*$^+$/HFD + PBS and *hIAPP*$^-$/HFD + PBS groups in **C** and **D**.)

steady-state autophagy level. Because the increase in the steady-state autophagy level could be due to either increased autophagy flux or blockade of autophagy at the lysosomal steps (29), we conducted Western blot analysis of pancreatic islets. Consistent with the increased autophagosome number, the LC3-II level was increased in islets of *hIAPP*$^{+/+}$ mice compared with that in those of *hIAPP*$^-$ mice (Supplemental Figure 3D). Here, we observed a markedly increased level of p62 protein in islets of *hIAPP*$^{+/+}$ mice (Supplemental Figure 3D), suggesting that p62, a specific substrate of autophagy (29), accumulated due to blockade of autophagy by hIAPP and that the increased LC3-II level is probably due to autophagy blockade rather than increased autophagic activity.

Effects of autophagy modulator on diabetes associated with hIAPP accumulation. Since the results suggested that autophagy insufficiency could be a risk factor in the pathogenesis of human T2D associated with hIAPP oligomer or amyloid deposition, we finally studied whether autophagy activation could ameliorate the metabolic profile of *hIAPP*$^+$ mice. To this end, we i.p. administered 2 g/kg trehalose, which has been reported to enhance autophagic activity in vivo (30, 31), to 16- to 20-week-old male *hIAPP*$^+$ mice with simultaneous high-fat diet (HFD) feeding to promote islet dysfunction and glucose intolerance (32, 33). The capability of trehalose to increase autophagic activity of pancreatic islet cells in vitro was confirmed by increased conversion of LC3-I to -II in the presence of bafilomycin, which blocks the lysosomal steps of autophagy and enables assessment of autophagic flux (ref. 29 and Figure 6A). Reduction of p62, a substrate of autophagy (29), by trehalose treatment in the absence of bafilomycin also supported increased autophagic flux in vitro (Figure 6A). Trehalose-induced activation of autophagy in pancreatic islets in vivo was also demonstrated by the apparently increased LC3 puncta after 2 weeks of trehalose administration to *GFP-LC3*$^+$ mice on a HFD compared with PBS treatment (Figure 6B).

When we analyzed the glucose profile, nonfasting blood glucose levels of PBS-treated HFD-fed *hIAPP*$^+$ mice without trehalose treatment were significantly higher compared with those of PBS-treated HFD-fed *hIAPP*$^-$ mice throughout the treatment period (P < 0.05~0.01), probably owing to β cell dysfunction associated with *hIAPP* expression (Figure 6C). Here, concomitant trehalose administration significantly reduced nonfasting blood glucose levels of HFD-fed *hIAPP*$^+$ mice, beginning at 1 week of treatment, compared with control PBS treatment (P < 0.05~0.01) (Figure 6C). Trehalose administration for 4 weeks significantly improved impaired glucose tolerance of HFD-fed *hIAPP*$^+$ mice (P < 0.05~0.01) (Figure 6D) and significantly decreased AUC and enhanced the insulinogenic index compared with control PBS treatment (P < 0.05~0.01) (Supplemental Figure 4A and Figure 6E). Glucose intolerance, AUC, and the insulinogenic index of PBS-treated HFD-fed *hIAPP*$^+$ mice were significantly worse compared with PBS-treated HFD-fed *hIAPP*$^-$ mice, probably due to β cell dysfunction associated with *hIAPP* expression (P < 0.05~0.001) (Figure 6, D and E; Supplemental Figure 4A). Changes in body weight during HFD feeding and food intake were not affected by trehalose administration (P > 0.1) (Supplemental Figure 4B and data not shown).

We also studied whether the observed metabolic improvement is accompanied by changes in hIAPP oligomer accumulation. Trehalose administration for 4 weeks significantly attenuated accumulation of A11-stained hIAPP oligomer in islets of HFD-fed *hIAPP*$^+$ mice compared with those given control treatment (P < 0.001) (Figure 6F), suggesting that metabolic improvement by trehalose administration is due to increased autophagic clearance of hIAPP oligomer, leading to enhanced β cell function. Accumulation of FSB-stained amyloid in islets of HFD-fed *hIAPP*$^+$ mice was also significantly reduced by trehalose administration for 4 weeks (P < 0.001) (Figure 6G).

Discussion

We observed the development of overt diabetes in mice with β cell–specific autophagy deficiency expressing amyloidogenic *hIAPP*, suggesting a critical role of autophagy in the turnover of hIAPP. Lysosomal proteolysis and autophagy have been reported to modulate hIAPP-induced cellular injury in vitro (34, 35). However, the role of autophagy in the development of hIAPP-induced diabetes in vivo has not been directly demonstrated. The development of overt diabetes in *hIAPP*$^+$*Atg7*$^{\Delta\beta cell}$ mice was due to increased β cell death, resulting in the critically reduced β cell mass and functional β cell impairment.

Such β cell injury appears to be caused by hIAPP oligomer accumulating in autophagy-deficient β cells, probably due to delayed clearance, which is consistent with our previous findings of oligomer-specific immunoreactivity and β cell apoptosis in islet cells of patients with T2D (36). A small amount of hIAPP amyloid was also observed in islets of *hIAPP*$^+$*Atg7*$^{\Delta\beta cell}$ mice. However, recent investigations suggest that the main effector of islet injury in *hIAPP*$^+$*Atg7*$^{\Delta\beta cell}$ mice is likely to be hIAPP oligomer (10, 18), which is supported by increased apoptosis of primary monkey islet cells expressing amyloidogenic *IAPP* together with I11-stained IAPP oligomer, but without amyloid accumulation when autophagy was inhibited in vitro. I11 Ab that is raised against hIAPP oligomer recognizes not only hIAPP oligomer but also Aβ oligomer. Conversely, A11 Ab that is raised against Aβ oligomer also recognizes hIAPP oligomer, suggesting a common conformational structure despite different amino acid sequences between hIAPP and Aβ peptides (17, 37). However, since recent papers reported A11 rec-

ognition of other proteins, such as natively folded heat shock proteins, binding specificities of I11 and A11 Ab may not be the same (38, 39). The mechanism of cellular damage by hIAPP oligomer is believed to be insertion into intracellular membranes and formation of ion-leaking pores (10, 40). Amyloidogenic hIAPP oligomer has also been shown to induce inflammasome activation (41, 42). While the role of inflammasome activation may not be significant in *hIAPP*$^{+}$*Atg7*$^{\Delta\beta cell}$ mice that show paucity of inflammatory cells in islets, islet inflammation may play an important role when conditions favoring further inflammasome activation, such as obesity or autophagy deficiency of macrophages, are superimposed (41).

p62 is a well-known autophagy receptor that guides autophagy substrates such as ubiquitinated proteins to LC3-II and is also a substrate of selective autophagy (43). While p62 binds to many target proteins of autophagic process, the absence of colocalization of hIAPP oligomer and p62 may suggest p62-independent autophagic removal of hIAPP oligomer, which is similar to a recently reported p62-independent autophagic clearance of aggregate-prone proteins, such as synphilin-1 (44). There may be autophagy receptors other than p62 involved in the autophagic removal of hIAPP oligomer, as diverse autophagic receptors, such as optineurin, NDP52, or NBR1, have been identified recently (45).

In our investigation of the clearance of hIAPP by autophagy, we observed pro-IAPP dimer in the soluble fraction of cell extract when amyloidogenic prepro-hIAPP was expressed in vitro but not when nonamyloidogenic prepro-mIAPP was expressed. Pro-hIAPP dimer formation was reduced markedly when the amino acid residues critical for fibril formation were changed to prolines as in pro-mIAPP (27). We further observed pro-hIAPP trimer in the detergent-insoluble fraction of cell extract under autophagy-deficient conditions. While hIAPP dimer formation has been observed in cell-free system (46) and hIAPP trimer formation has been inferred using molecular dynamic simulation studies (47, 48), the formation of hIAPP or pro-hIAPP dimer and trimer has not been demonstrated in cells. Accumulation of pro-hIAPP dimer or trimer might be due to pro-hIAPP overexpression exceeding the cell's capacity to process pro-hIAPP to mature form. The role of aberrant or incomplete processing of hIAPP in the development of hIAPP amyloid has been suggested by previous findings that conditions favoring aberrant proinsulin processing, such as T2D or insulinoma, are frequently associated with amyloid deposition (49, 50) and that the expression of *hIAPP* in cells defective in hIAPP processing results in increased amyloid formation (24, 26). Furthermore, pro-hIAPP immunoreactivity has been demonstrated in the intracellular amyloid of β cells in *hIAPP*$^{+}$ mice or patients with T2D, suggesting that intracellular aggregation of pro-hIAPP is the initial step acting as the seed for further amyloidogenesis and extracellular amyloid deposition in the later stage in conjunction with mature IAPP released from β cells (25).

The propensity of pro-hIAPP to aggregate may be related to the biochemical characteristics of pro-hIAPP, such as a higher PI value compared with mature IAPP, and the presence of a heparin binding domain in the N-terminal cleavage site that may facilitate its association with negatively charged membranes and the initiation of amyloidogenesis (25, 51, 52). Thus, our results showing the existence of intracellular pro-hIAPP dimer or trimer in vitro suggest that low-*n* pro-hIAPP oligomers may be the initial starting point ultimately leading to the formation of high-*n* hIAPP oligomers and hIAPP amyloid. In contrast, other reports have suggested the hexameric structure of amyloidogenic peptides as the basic toxic oligomer species recognized by oligomer-specific Ab (53). Details regarding possible interconversion between these different oligomer species warrant further studies.

Markedly increased accumulation of pro-hIAPP dimer in autophagy-deficient β cells and the presence of pro-hIAPP trimer in the detergent-insoluble fraction of autophagy-deficient β cells are consistent with results from previous reports that aggregate-prone proteins are cleared preferentially by autophagy compared with nonaggregate-prone proteins (11). These results also suggest that the critical point in the maturation of high-*n* hIAPP oligomers could be the formation of pro-hIAPP dimer and trimer, probably in the membrane-rich fraction of the cells. This hypothesis is in line with a previous suggestion that the initial stage of islet amyloid deposition would be the formation of hIAPP aggregates containing pro-hIAPP in the membrane compartment of cells (10). Recent molecular dynamic approaches indicated that there is a significant stability gained during the transition from hIAPP dimer to trimer and that hIAPP trimer is the minimal oligomeric size of an aggregate seed that is required for the formation of stable hIAPP oligomer, suggesting the importance of hIAPP trimer formation in the maturation of high-*n* hIAPP oligomers, while dimer formation might be the initial step in the maturation process (47, 48). As pro-hIAPP trimer was found in the detergent-insoluble fraction and the amount of pro-hIAPP dimer was much higher in the detergent-insoluble fraction compared with that in the detergent-soluble fraction, pro-hIAPP dimer is likely to be formed in the membrane-rich compartment, such as secretory granules, and is translocated to the soluble fraction or proceeds to form pro-hIAPP trimer in the membrane-rich fraction (Figure 7). Such a scenario is consistent with previous reports that the lipid membrane is a catalytic site for hIAPP misfolding to accelerate protein aggregation (54) and has a facilitated association with pro-hIAPP (26, 52). While we observed accumulation of pro-hIAPP dimer and trimer as a potential seed for high-*n* hIAPP oligomer formation, we cannot eliminate the possibility that other hIAPP forms, such as mature or partially processed forms, also oligomerize. Thus, our data support a role for pro-hIAPP oligomerization in the current overexpression model but do not rule out other possibilities.

While hIAPP oligomer was cleared by autophagy, *hIAPP* expression conversely appeared to block autophagic flux, as Western blot analysis demonstrated that p62 levels were increased in islets of *hIAPP*$^{+/+}$ mice. In contrast, p62 accumulation was virtually absent in islets of heterozygous *hIAPP*$^{+}$*Atg7*$^{fl/fl}$ mice by confocal microscopy, probably owing to lower hIAPP expression levels. These results supporting autophagy blockade by hIAPP in vivo are consistent with the previously reported inhibition of autophagic flux by *hIAPP* overexpression in vitro (35) and are similar to the suppression of autophagic flux at the lysosomal step in the brain of Alzheimer's disease (55). These results suggest that if autophagic activity is reduced to a threshold level, then amyloidogenic proteins accumulate and further impair autophagic activity. This series of events would result in a positive-feedback loop and lead to critically reduced autophagic activity, cellular damage due to accumulated amyloidogenic proteins, and finally the development of diabetes or Alzheimer's disease.

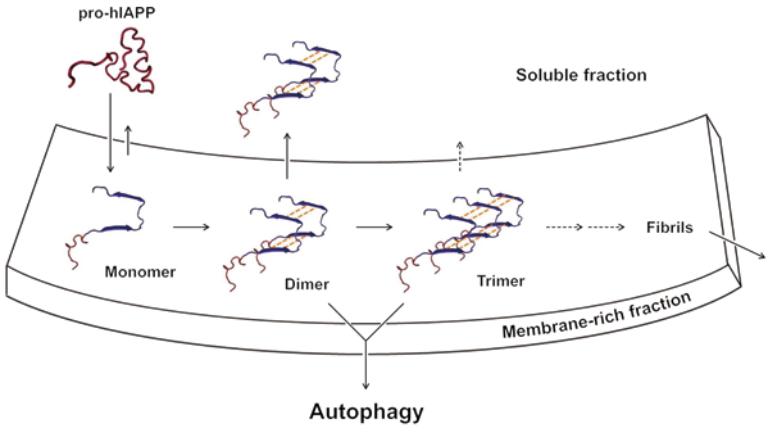

Figure 7. Proposed model of pro-hIAPP dimer and trimer formation. The site of pro-hIAPP dimerization would be the membrane-rich fraction rather than the soluble fraction, since, after binding of pro-hIAPP to the membrane fraction, the local concentration of pro-hIAPP will increase and the encounter between molecules will be restricted to 2 dimensions (54). Some of the pro-hIAPP dimer will be translocated to the soluble fraction, while other pro-hIAPP dimer would proceed to form pro-hIAPP trimer, probably in the membrane-rich fraction. Although the exact molecular structure of the pro-hIAPP trimer is unknown, a recently proposed parallel stacking model with a U-bend conformation of β-strand–loop–β-strand (47, 62) is shown.

To investigate the impact of autophagy enhancers on the deteriorated metabolic profile associated with hIAPP accumulation, we used *hIAPP*$^+$ mice fed HFD, since HFD imposes metabolic stress and β cell dysfunction on *hIAPP*$^+$ mice (32, 33) and lipid injury can further impair autophagic activity of pancreatic β cells (56). To enhance autophagic activity in vivo, we used trehalose instead of rapamycin, a well-known autophagy enhancer (29), because trehalose has been reported to improve neurologic deficit by enhancing autophagic activity in vivo (30, 31) and rapamycin has adverse metabolic effects (57, 58). Indeed, we found that trehalose increased autophagic activity of islet cells in vitro and in vivo. Strikingly, trehalose significantly improved the metabolic profile of *hIAPP*$^+$ mice on HFD, which was accompanied by enhanced β cell function and attenuated hIAPP oligomer accumulation. To our knowledge, the ability of trehalose to improve the metabolic profile by enhancing autophagic activity has not been reported. These results imply promising therapeutic potential of trehalose against human T2D associated with islet amyloid deposition or that with reduced autophagic activity due to aging, obesity, or genetic predisposition.

Altogether, these results suggest that amyloidogenic hIAPP protein is cleared by autophagy and autophagy deficiency leads to accumulation of hIAPP oligomer and deposition of amyloid that are distinct from inclusion bodies observed in autophagy-deficient cells and comprise nonamyloidogenic proteins. Cellular injury, likely mediated by hIAPP oligomer, would lead to β cell death and functional impairment of β cells, such as diminished Ca^{2+} transients or insulin release in response to glucose. Autophagy deficiency associated with genetic predisposition or aging could be a factor in the development of human diabetes, in which accumulation of amyloidogenic hIAPP is observed frequently in contrast to murine diabetes. Novel agents such as trehalose that can enhance autophagic activity without adverse metabolic effects could be a future strategy for treatment of human T2D.

Methods

Animals. RIP-*Cre* mice of C57BL/6 background (Jackson Laboratory) were bred with *Atg7*$^{fl/fl}$ mice of C57BL/6 background and then with *hIAPP*$^+$ mice (Jackson Laboratory) to finally generate *hIAPP*$^+$*Atg7*$^{\Delta\beta cell}$ mice at the second intercross generation. *hIAPP*$^+$ mice were maintained on FVB/N background. RIP-*Cre* and *Atg7*$^{fl/fl}$ mice were genotyped as previously reported (5, 16). The presence of *hIAPP* transgene was confirmed by PCR analysis of tail DNA using specific primers (forward, 5′-GTCATGTGCACCTAAAGGGGCAAGTAATTCA-3′; reverse, 5′-CGAGTGGGCTATGGGTTTGT-3′). IPGTT was conducted by i.p. injection of 1 g/kg glucose to mice that were fasted overnight. Blood glucose concentration was measured using a One Touch glucometer (Lifescan) (5, 16). To generate *hIAPP*$^+$*GFP-LC3*$^+$ mice, *GFP-LC3*$^+$ mice (provided by N. Mizushima, University of Tokyo, Tokyo, Japan) were bred with *hIAPP*$^+$ mice. *hIAPP*$^+$*GFP-LC3*$^+$ mice were bred with *hIAPP*$^+$ mice again to generate homozygous *hIAPP*$^{+/+}$*GFP-LC3*$^+$ mice. *hIAPP*$^{+/+}$ mice were generated by intercrossing *hIAPP*$^+$ mice. Homozygous *hIAPP*$^{+/+}$ mice were identified by backcrossing to nontransgenic FVB/N mice (13).

Cynomolgus monkeys were purchased from Guangxi Grandforest Scientific Primate Company Ltd. and maintained in Orientbio Animal Facility.

Cells. INS-1 cells (provided by C. Wollheim, University of Geneva, Geneva, Switzerland) were cultured in RPMI-1640 supplemented with 10% FCS, 1 mM sodium pyruvate, 10 mM HEPES, 50 μM 2-mercaptoethanol, and penicillin-streptomycin (Life Technologies).

TUNEL staining, β cell mass, and function. Quantitation of TUNEL$^+$ apoptotic β cells was done as described previously (5). Briefly, deparaffinized pancreas sections were stained using TUNEL reagent (Roche Applied Science) and DAB (Invitrogen) as the color substrate. Insulin immunostaining was then performed by serial incubation with anti-insulin Ab (DAKO), biotinylated anti-guinea pig Ab (Vector), streptavidin-alkaline phosphatase, and then Vector Blue (Vector) staining solution. In each group, 5,024~9,206 β cells from 4~5 mice were examined. To calculate the relative β cell mass, point counting morphometry was performed after insulin IHC of more than 3 parallel sections of different cut levels containing more than 30 pancreatic islets (5, 16). Serum insulin levels before and 15 minutes after glucose challenge were determined using an ELISA kit (Shibayagi Co.), and the insulinogenic index was calculated as follows: ($\Delta insulin_{15min}$/$\Delta glucose_{15min}$) (5, 16).

IAPP expression in vitro. 5′-phosphorylated synthetic oligos encoding HA epitope ("YPYDVPDYA") were annealed and inserted directly into unique HindIII and Eco0109I sites of pcDNA5-FRT/TO (pcDNA5-FRT/TO-HA). cDNAs encoding prepro-hIAPP (Genebank accession number: NM 000415) and prepro-mIAPP (NM 010491) in pcDNA3 were gifts from P. Westermark (Uppsala University, Uppsala, Sweden). The cDNA was PCR amplified using the following specific primers: prepro-hIAPP forward-HindIII, 5′-CTTAAGCTTACCATGGGCATCCTGAAGCTGCAAG-3′; reverse-XhoI, 5′-CCGCTCGAGCTAAAGGGGCAAGTAATTCAG-3′; prepro-mIAPP forward-HindIII,

5′-CTTAAGCTTACCATGTGCATCTCCAAAC-3′; reverse-XhoI, 5′-CCGCTCGAGTTAAACGAGTAAGAAATCCAAG-3′ (restriction sites are underlined). After digestion with HindIII and Xho, PCR products were subcloned into pcDNA5-FRT/TO-HA to produce prepro-hIAPP-HA and prepro-mIAPP-HA. Mutant prepro-hIAPP was generated by changing codons for Ala at codon 58 (GCC) and for Ser at codon 61 (TCA) and 62 (TCT) to the codons for Pro (CCA) by site-directed mutagenesis using the following synthetic oligonucleotides: prepro-hIAPP^{mt} forward, 5′-AGCAACAACTTTGGTCCAATTCTCCCACCAACCAACGTGGGATCC-3′; reverse, 5′-GGATCCCACGTTGGTTGGTGGGAGAATTGGACCAAAGTTGTTGCT-3′ (codons for proline are underlined). Site-directed mutagenesis of the cleavage site of "pre" sequence from prepro-IAPP (A23D mutation of prepro-mIAPP-HA and A22D mutation of prepro-hIAPP-HA) was conducted in a similar way. Transient transfection was performed using Effectene (Qiagen) (for monkey islet cells or INS-1 cells) or jetPEI DNA transfection reagent (Polyplus) (for INS-1 cells) according to the manufacturer's instructions.

To block autophagy of transfected cells, after 24 hours of transfection, culture medium was changed to a new medium containing 5 mM 3-MA for INS-1 cells or containing 100 nM bafilomycin for primary islet cells. After another 24 hours of incubation, cells were lysed with a lysis buffer (150 mM NaCl, 50 mM Tris-HCl, pH 7.4, 50 mM HEPES, 0.5% Triton X-100, and 0.5% deoxycholate). For some experiments, cell lysates were further separated into soluble and insoluble fractions by centrifugation at 8,000 *g* for 30 minutes. The detergent-soluble fraction was loaded onto a gel and separated electrophoretically. Detergent-insoluble pellets were fully solubilized in the original volume of 1% SDS, 100 mM Tris, pH 7.5, and separated electrophoretically.

Western blotting. Western blot analysis was done using Abs specific for LC3 (Novus), p62 (Progen), HA (Cell Signaling), or β-actin (Santa Cruz) after separation on a gradient gel (NuPAGE, Life Technology).

Confocal microscopy. Expression of p62, ubiquitin, and insulin was evaluated by confocal microscopy (Carl Zeiss) after immunofluorescent staining of deparaffinized tissue sections. Accumulation of hIAPP oligomer in frozen tissue sections or cells cultured in Lab-Tak II Chamber Slide (Thermo) was studied the same way. GFP fluorescence in islets of *GFP-LC3*$^{+}$ mice was also examined by confocal microscopy. Line tracing, a method of tracking signal intensities along arbitrary lines, was conducted to examine colocalization of color signals. The following primary Abs were used confocal microscopy: anti-insulin, anti-ubiquitin (DAKO), anti-p62 (Progen), I11 (provided by C.G. Glabe, UC Irvine, Irvine, California, USA), and A11 (Millipore). Secondary Abs were from Invitrogen.

Amyloid staining. Deparaffinized sections or cells cultured in chamber slides were treated with 70% formic acid for 20 minutes and then incubated with 1% Thioflavin-S (Sigma-Aldrich) at room temperature, with light protection for 20 minutes or with 10 μM FSB (Millipore) for 1 hour. Cells were mounted after counterstaining with DAPI for observation on a fluorescent microscope (Nikon).

Isolation of pancreatic islets. Murine islets were isolated from fasted mice using the collagenase digestion technique as described previously (59). Briefly, the pancreas was procured after injection of 2.5 ml collagenase P (0.8 mg/ml) into the bile duct and incubated in collagenase solution at 37°C for 13 minutes and 20 seconds with gentle shaking. After termination of enzymatic digestion with cold HBSS-5% FCS, tissue was passed through a 400-μm sieve and centrifuged on 1.10, 1.085, 1.069, and 1.037 g/ml Biocoll gradients (Biochrom). Islets were collected from the interface, and individual islets were hand-picked using micropipettes. Collected islets were then dissociated into single cells by incubation with trypsin-EDTA for 5 minutes.

Primary monkey islet cells were isolated using the modified Ricordi's method (60). Briefly, pancreata were dissected from 60-month-old male monkeys and placed in 4°C HTK solution, followed by distention with 3~4 ml/g pancreas cold Liberase MTF C/T solution (Roche). The distended pancreas was placed in an isolation chamber equipped with a peristaltic pump, and the temperature was raised to 37°C. During digestion, the isolation chamber was gently shaken, and serial samples were examined by light microscopy after dithizone (Sigma-Aldrich) staining. When free islets were observed, Dilution Solution (Corning) was applied to inactivate Liberase MTF C/T. Digested cells were collected into 200-ml conical tubes and washed with Washing Solution (Corning). Islets were then isolated by continuous density gradient centrifugation using a COBE 2991 Cell Processor (COBE BCT Inc.) in a solution containing iodixanol (Optiprep, Axis-Shield). Collected islets were counted and cultured in CMRL1066 medium supplemented with 10% FCS at 37°C.

RT-PCR. RNA was prepared from isolated islet cells using TRIzol Reagent (Ambion). cDNA was synthesized using M-MLV Reverse Transcriptase (Promega) and oligo(dT)$_{12-18}$ primer. The expression of *Atg7* and *hIAPP* was examined by RT-PCR using specific primers (*hIAPP* forward, 5′-CCTGAAGCTGCAAGTATTTC-3′; reverse, 5′-TTGGTAGATGAGAGAATGGC-3′; *Atg7* forward, 5′-TGTGGAGCTGATGGTCTCTG-3′; reverse, 5′-TGATGGAGCAGGGTAAGACC-3′; β-actin forward, 5′-AGAGGGAAATCGTGCGTGACA-3′; reverse, 5′-CACTGTGTTGGCATAGAGGTC-3′).

Measurement of $[Ca^{2+}]_c$. $[Ca^{2+}]_c$ was measured as described previously with modifications (59). Briefly, medium-sized islets were loaded with 4 μM Fura 2-AM for 30 minutes at room temperature. After washing twice with Tyrode solution, $[Ca^{2+}]_c$ was recorded using a microfluorometric system comprising an inverted fluorescence microscope (Olympus) equipped with a dry-type fluorescence objective lens, a photomultiplier tube (Hamamatsu), and a Deltascan illuminator (Photon Technology International). $[Ca^{2+}]_c$ was calculated from the fluorescence emission ratio at 340 nm/380 nm excitation. $\Delta[Ca^{2+}]_c$ area was calculated as the total area of $[Ca^{2+}]_c$ above the basal $[Ca^{2+}]_c$.

Islet cell death. Primary pancreatic islets were placed on Tissue Culture Testplate (SPL Life Science) and incubated with 100 nM bafilomycin (Sigma-Aldrich) for 24 hours. Apoptosis was quantified by measuring the amount of oligonucleosomes in cell lysate by ELISA using a Cell Death Detection ELISA Kit (Roche), according to the manufacturer's instruction.

EM. Ultrastructural changes of cells at the organelle level were examined using EM, and the number of autophagosomes was counted as described previously (5). Double-membrane compartments containing loose cytoplasmic material or organelles were considered autophagosomes (61).

Trehalose treatment. While 16- to 20-week-old *hIAPP*$^{+}$ mice were fed HFD, 2 g/kg trehalose (Sigma-Aldrich) dissolved in PBS was administered i.p. 3 times a week. IPGTT was performed after trehalose administration for 4 weeks, and the AUC and insulinogenic index were calculated. For in vitro treatment, primary murine islet cells were treated with 100 mM trehalose for 24 hours with or without 100 nM bafilomycin pretreatment, and cell lysates were subjected to Western blot analysis using anti-LC3, anti-p62, or anti–β-actin Ab.

Statistics. All values are expressed as mean ± SD. A 2-tailed Student's *t* test was used to compare the values between groups. *P* values less than 0.05 were considered significant.

Study approval. All animal experiments were conducted in accordance with the Public Health Service Policy on Humane Care and Use of Laboratory Animals. Mouse experiments were approved by the IACUC of Samsung Medical Center Animal Facility, an Association for Assessment and Accreditation of Laboratory Animal Care–accredited (AAALAC-accredited) unit. Monkey experiments were approved by the IACUC of Orientbio, another AAALAC-accredited unit.

Acknowledgments

This study was supported by the Global Research Laboratory Grant of the National Research Foundation of Korea (K21004-000003-12A0500-00310). We thank K. Cho for caring for monkeys at Orientbio and J.B. Park and S.J. Kim for technical support in the isolation of primary monkey islet cells. We are grateful to K. Eom for the suggestion about the structure of hIAPP oligomer.

Address correspondence to: Myung-Shik Lee, Department of Medicine, Samsung Medical Center, Sungkyunkwan University School of Medicine, 81 Irwon-ro, Gangam-gu, Seoul, Republic of Korea. Phone: 82.2.3410.3436; E-mail: mslee0923@skku.edu. Or to: Sang-Wook Kang, Department of Biomedical Sciences, University of Ulsan, 88 Olympic-ro 43-gil, Songpa-gu, Seoul, Republic of Korea. Phone: 82.2.3010.2205; E-mail: swkang@amc.seoul.kr.

1. Klionsky DJ, Emr SD. Autophagy as a regulated pathway of cellular degradation. *Science*. 2000;290(5497):1717–1721.
2. Levine B, Yuan J. Autophagy in cell death: an innocent convict? *J Clin Invest*. 2005;115(10):2679–2688.
3. Kahn SE. The relative contribution of insulin resistance and beta-cell dysfunction to the pathophysiology of type 2 diabetes. *Diabetologia*. 2003;46(1):3–19.
4. Ebato C, et al. Autophagy is important in islet homeostasis and compensatory increase of beta cell mass in response to high-fat diet. *Cell Metab*. 2008;8(4):325–332.
5. Jung HS, et al. Loss of autophagy diminishes pancreatic β-cell mass and function with resultant hyperglycemia. *Cell Metab*. 2008;8(4):318–324.
6. Kim KH, et al. Autophagy deficiency leads to protection from obesity and insulin resistance by inducing FGF21 as a 'mitokine'. *Nat Med*. 2013;19(1):83–92.
7. Singh R, et al. Autophagy regulates lipid metabolism. *Nature*. 2009;458(7242):1131–1135.
8. Yang L, Li P, Fu S, Calay ES, Hotamisligil GS. Defective hepatic autophagy in obesity promotes ER stress and causes insulin resistance. *Cell Metab*. 2010;11(6):467–478.
9. Kahn SE, Andrikopoulos S, Verchere CB. Islet amyloid: a long-recognized but underappreciated pathological feature of type 2 diabetes. *Diabetes*. 1999;48(2):241–253.
10. Westermark P, Andersson A, Westernark GT. Islet amyloid polypeptide, islet amyloid, and diabetes mellitus. *Physiol Rev*. 2011;91(3):795–826.
11. Rubinsztein DC. The roles of intracellular protein-degradation pathways in neurodegeneration. *Nature*. 2006;443(7113):780–786.
12. Höppener JW, et al. Extensive islet amyloid formation is induced by development of type II diabetes mellitus and contributes to its progression: pathogenesis of diabetes in a mouse model. *Diabetologia*. 1999;42(4):427–434.
13. Janson J, et al. Spontaneous diabetes mellitus in transgenic mice expressing human islet amyloid polypeptide. *Proc Natl Acad Sci U S A*. 1996;93(14):7283–7288.
14. Verchere CB, D'Alessio DA, Palmiter RD, Kahn SE. Transgenic mice overproducing islet amyloid polypeptide have increased insulin storage and secretion in vitro. *Diabetologia*. 1994;37(7):725–728.
15. Verchere CB, et al. Islet amyloid formation associated with hyperglycemia in transgenic mice with pancreatic beta cell expression of human islet amyloid polypeptide. *Proc Natl Acad Sci U S A*. 1996;93(8):3492–3496.
16. Han MS, et al. Imatinib mesylate reduces endoplasmic reticulum stress and induces remission of diabetes in db/db mice. *Diabetes*. 2009;58(2):329–336.
17. Kayed R, et al. Fibril specific, conformation dependent antibodies recognize a generic epitope common to amyloid to amyloid fibrils and fibrillar oligomers that is absent in prefibrillar oligomers. *Mol Neurodegener*. 2007;2:18.
18. Haataja L, Gurlo T, Huang CJ, Butler PC. Islet amyloid in type 2 diabetes, and the toxic oligomer hypothesis. *Endocr Rev*. 2008;29(3):303–316.
19. Mizushima N, Yamamoto A, Matsui M, Yoshimori T, Ohsumi Y. In vivo analysis of autophagy in response to nutrient starvation using transgenic mice expressing a fluorescent autophagosome marker. *Mol Biol Cell*. 2004;15(3):1101–1111.
20. Lin CY, et al. Toxic human islet amyloid polypeptide (h-IAPP) oligomers are intracellular, and vaccination to induce anti-toxic oligomer antibodies does not prevent h-IAPP-induced beta-cell apoptosis in h-IAPP transgenic mice. *Diabetes*. 2007;56(5):1324–1332.
21. Sato K, Higuchi M, Iwata N, Saido TC, Sasamoto K. Fluoro-substituted and 13C-labled styrylbenzene derivatives for detecting brain amyloid plaques. *Eur J Med Chem*. 2004;39(7):573–578.
22. Skovronsky DM, et al. In vivo detection of amyloid plaques in a mouse model of Alzheimer's disease. *Proc Natl Acad Sci U S A*. 2000;97(13):7609–7614.
23. O'Brien TD, et al. Islet amyloid and islet amyloid polypeptide in cynomolgus macaques (Macaca fascicularis): an animal model of human non-insulin-dependent diabetes mellitus. *Vet Pathol*. 1996;33(5):479–485.
24. Marzban L, et al. Impaired NH2-terminal processing of human proislet amyloid polypeptide by the prohormone convertase PC2 leads to amyloid formation and cell death. *Diabetes*. 2006;55(8):2192–2201.
25. Paulsson JF, Anderson A, Westermark P, Westermark GT. Intracellular amyloid-like deposits contains unprocessed pro-islet amyloid polypeptide (proIAPP) in β cells of transgenic mice overexpressing the gene for human IAPP and transplanted human islet. *Diabetologia*. 2006;49(6):1237–1246.
26. Paulsson JF, Westermark GT. Aberrant processing of human proislet amyloid polypeptide results in increased amyloid formation. *Diabetes*. 2005;54(7):2117–2125.
27. Westermark P, Engström U, Johnson KH, Westermark GT, Betsholtz C. Islet amyloid polypeptide: pinpointing amino acid residues linked to amyloid fibril formation. *Proc Natl Acad Sci U S A*. 1990;87(13):5036–5040.
28. Liu M, et al. Impaired cleavage of preproinsulin signal peptide linked to autosomal-dominant diabetes. *Diabetes*. 2012;61(4):828–837.
29. Klionsky DJ, et al. Guidelines for the use and interpretation of assays for monitoring autophagy. *Autophagy*. 2012;8(4):445–544.
30. Rodriguez-Navarro JA, et al. Trehalose ameliorates dopaminergic and tau pathology in parkin deleted/tau overexpressing mice through autophagy activation. *Neurobiol Dis*. 2010;39(3):423–438.
31. Sarkar S, Davies JE, Huang Z, Tunnacliffe A, Rubinsztein DC. Trehalose, a novel mTOR-independent autophagy enhancer, accelerates the clearance of mutant huntingtin and a-synuclein. *J Biol Chem*. 2007;282(8):5641–5652.
32. Hull RL, et al. Increased dietary fat promotes islet amyloid formation and β-cell secretory dysfunction in a transgenic mouse model of islet amyloid. *Diabetes*. 2003;52(2):372–379.
33. Matveyenko AV, Gurlo T, Daval M, Butler AE, Butler PC. Successful versus failed adapation to high-fat diet-induced insulin resistance: the role of IAPP-induced β-cell endoplasmic reticulum stress. *Diabetes*. 2009;58(4):906–916.
34. Morita S, et al. Autophagy protects against human islet amyloid polypeptide-associated apoptosis. *J Diabetes Invest*. 2011;2(1):48–55.
35. Rivera JF, et al. Human-IAPP disrupts the autophagy/lysosomal pathway in pancreatic β-cells: protective role of p62-postivie cytoplasmic inclusions. *Cell Death Differ*. 2011;18(3):415–426.
36. Park JY, et al. Pathologic changes and glucose homeostasis according to expression of human islet amyloid polypeptide in type 2 diabetic patients.

J Histochem Cytochem. 2010;58(8):731–740.
37. Kayed R, et al. Common structure of soluble amyloid oligomers implies common mechanism of pathogenesis. *Science*. 2003;300(5618):486–489.
38. Yoshiike Y, et al. Amyloid oligomer conformation in a group of natively folded proteins. *PLoS ONE*. 2008;3(9):e3235.
39. Zraika S, et al. Toxic oligomers and islet beta cell death: guilty by association of convicted by circumstantial evidence? *Diabetologia*. 2010;53(6):1046–1056.
40. Janson J, Ashley RH, Harrison D, McIntyre S, Butler PC. The mechanism of islet amyloid polypeptide toxicity is membrane disruption by intermediate-sized toxic amyloid particles. *Diabetes*. 1999;48(3):491–498.
41. Masters SL, et al. Activation of the NLRP3 inflammasome by islet amyloid polypeptide provides a mechanism for enhanced IL-1b in type 2 diabetes. *Nat Immunol*. 2010;11(10):897–904.
42. Westwell-Roper C, et al. IL-1 blockade attenuates islet amyloid polypeptide-induced proinflammatory cytokine release and pancreatic islet graft dysfunction. *J Immunol*. 2011; 187(5):2755–2765.
43. Komatsu M, et al. Homeostatic levels of p62 control cytoplasmic inclusion body formation in autophagy-deficient mice. *Cell*. 2007;131(6):1149–1163.
44. Wong E, et al. Molecular determinants of selective clearance of protein inclusions by autophagy. *Nat Commun*. 2012;3:1240.
45. Birgisdottir AB, Lamark T, Johansen T. The LIR motif-crucial for selective autophagy. *J Cell Sci*. 2013;126(pt 15):3237–3247.
46. Dupuis NF, Wu C, Seha J-M, Bowers MT. The amyloid formation mechanism in human IAPP: dimers have β-strand monomer-monomer interfaces. *J Am Chem Soc*. 2011;133(19):7240–7243.
47. Liang G, Zhao J, Yu X, Zheng J. Comparative molecular dynamics study of human islet amyloid polypeptide (IAPP) and rat IAPP oligomers. *Biochemistry*. 2013;52(6):1089–1100.
48. Mo Y, Wei G, Derreumaux P. Structural diversity of the soluble trimers of the human amylin(20-29) peptide revealed by molecular dynamics simulations. *J Chem Phys*. 2009;130(12):125101.
49. Kahn SE, Halban PA. Release of incompletely processed proinsulin is the cause of disproportionate proinsulinonemia of NIDDM. *Diabetes*. 1997;46(11):1725–1732.
50. O'Brien TD, Butler AE, Roche PC, Johnson KH, Butler PC. Islet amyloid polypeptide in human insulinomas. Evidence for intracellular amyloidogenesis. *Diabetes*. 1994;43(2):329–336.
51. Jayasinghe SA, Langen R. Lipid membranes modulate the structure of islet amyloid polypeptide. *Biochemistry*. 2005;44(36):12113–12119.
52. Park K, Verchere CB. Indentification of a heparin binding domain in the N-terminal cleavage site of pro-islet amyloid polypeptide. *J Biol Chem*. 2001;276(20):16611–16616.
53. Laganowsky A, et al. Atomic view of a toxic amyloid small oligomer. *Science*. 2012;335(6073):1228–1231.
54. Apostolidou M, Jayasinghe SA, Langen R. Structure of a-helical membrane-bound human islet amyloid polypeptide and its implication for membrane-mediated folding. *J Biol Chem*. 2008;283(25):17205–17210.
55. Nixon RA. Autophagy, amyloidogenesis and Alzheimer disease. *J Cell Sci*. 2007; 120(pt 23):4081–4091.
56. Quan W, et al. Autophagy deficiency in beta cells leads to compromised unfolded protein response and progression from obesity to diabetes in mice. *Diabetologia*. 2012;55(2):392–403.
57. Fraenkel M, et al. mTOR inhibition by rapamycin prevents beta-cell adaptation to hyperglycemia and exacerbates the metabolic state in type 2 diabetes. *Diabetes*. 2008;57(4):945–957.
58. Sarbessov DD, et al. Prolonged rapamycin treatment inhibits mTORC2 assembly and Akt/PKB. *Mol Cell*. 2006;22(2):159–168.
59. Chang I, et al. Role of calcium in pancreatic islet cell death by IFN-γ/TNF-α. *J Immunol*. 2004;172(11):7008–7014.
60. Ricordi C, Lacy PE, Finke EH, Olack B, Scharp DW. Automated method for the isolation of human pancreatic islets. *Diabetes*. 1988;37(4):413–420.
61. Boland B, et al. Autophagy induction and autophagosome clearance in neurons: relationship to autophagic pathology in Alzheimer's disease. *J Neurosci*. 2008;28(27):6926–6937.
62. Luca S, Yau W-M, Leapmen R, Tycko R. Peptide conformation and supramolecular organization in amylin fibril: constraints from solid-state NMR. *Biochemistry*. 2007;46(47):13505–13522.